Investigation of the Electronic Crosstalk in Terra MODIS Band 28

Junqiang Sun[1,2], Sriharsha Madhavan[3], Xiaoxiong Xiong[4], and Menghua Wang[1]

[1]NOAA National Environmental Satellite, Data, and Information Service
Center for Satellite Applications and Research
E/RA3, 5830 University Research Ct., College Park, MD 20740, USA

[2]Global Science and Technology, 7855 Walker Drive, Suite 200, Greenbelt, MD 20770, USA

[3]Science and Systems Applications Inc, 10210, Greenbelt Road, Lanham, MD 20706
[4]Sciences and Exploration Directorate, NASA/GSFC, Greenbelt, MD 20771

ABSTRACT

The Moderate Resolution Imaging Spectroradiometer (MODIS) is a whisk broom scanning radiometer which is on board the Terra and Aqua spacecraft. Both MODIS instruments have successfully completed more than twelve years of on-orbit flight. The Long Wave Infrared (LWIR) Photovoltaic (PV) bands (bands 27-30, 6.72-9.73 μm) on the LWIR Focal Plane Assembly (FPA) in Terra MODIS have contamination due to electronic crosstalk.. In this paper, we examine Terra MODIS band 28 (7.33 μm) crosstalk effects, their impact, and mitigation. The crosstalk signal is identified and characterized using the regular lunar observations acquired by MODIS. It is evident from the derived crosstalk coefficients that the contamination was mainly from bands 27 (6.72 μm), 29 (8.55 μm), and 30 (9.73 μm). The crosstalk coefficients are generally a small positive quantity in the early to middle part of the mission with a few exceptions, and then changing directions. A linear correction algorithm is applied to both L1B calibration and retrieval to qualitatively and quantitatively assess the impact and improvements in this paper. It is shown that the crosstalk correction improved the imagery and radiometric fidelity of this band.

Keywords: MODIS, Moon, Crosstalk, Terra, Thermal emissive bands, Striping, Radiometric improvements

1. INTRODUCTION

Terra, one of the prime platforms for NASA's Earth Observing System (EOS) [1-4], has an equatorial crossing time of approximately 10:30 am. The Terra spacecraft has successfully completed 14 years of on orbit flight as of 17 December 2013. The MODIS remotely collects information in 36 spectral bands varying from about 0.4 μm to 14.4 μm of which wavelengths from 3.7 μm onwards cover the thermal infrared region. The MODIS instrument is a cross track whisk broom scanning radiometer, which has a 360 degree rotating double-sided scan mirror, with several On Board Calibrators (OBC). The four bands 27-30 (6.72-9.73 μm) comprise the long wave infrared (LWIR) photo voltaic (PV) bands, whose location on the MODIS LWIR Focal Plane Assembly (FPA) is shown in Figure 1, and have a radiometric calibration

uncertainty requirement of 1% [5]. The band focused in this paper is Terra MODIS band 28 (center wavelength of approximately 7.33 μm) whose primary use is in measuring water vapor distribution and detection of volcanic cloud components. The MODIS Thermal Emissive Bands (TEB) are calibrated through the on-board Blackbody (BB) and via the Space View (SV) port on a scan by scan basis, thus providing high fidelity tracking of the on-orbit gain changes for the instrument [6]. In recent years (2010 onwards), the PV LWIR bands have indicated a noisy response as monitored by the Noise Equivalent Temperature difference (NEdT) trends. In addition, the corresponding instrument gain (calibration coefficients) trends for these noisy detectors are marked with sudden changes. Through the various instrument settings of detector voltage and currents performed early in mission, electronic crosstalk was found to be a significant contributor to the sudden changes in the response of the detectors [7]. Previous electronic crosstalk studies in other MODIS bands such as band 27 (6.72 μm) also had indicated a crosstalk among different bands and the crosstalk effect is strongly detector-dependent. Hence, a careful probe using the lunar observations was done in the case of band 28 and similar effect was found. However, there were differences in the nature of crosstalk. First, the magnitude of crosstalk signal was slightly smaller for band 28 in comparison to band 27. Second, band 27 imagery contained ghosting ground features in addition to the striping contamination [7]. Unlike in band 27, the ghosting effect in band 28 was minimal which was mainly due to the different amount of ground feature (corresponds to the crosstalk signal) observed from the spectral wavelengths of the two bands. However, the similarity of the crosstalk contamination in both bands 27 and 28 was the predominant striping feature due to the detector-to-detector response differences. These differences are mainly due to the crosstalk from other PV LWIR bands, which will be discussed in greater detail in the following sections.

The rest of the paper is organized as follows. Section 2 describes the electronic crosstalk phenomena as observed from Earth View (EV) images and through the on board lunar measurements. The nature of crosstalk impact is understood by analyzing the response profiles in the horizontal and vertical directions of the EV imagery. The section also focuses on understanding the magnitude of leak and the associate impact. Section 3 describes the crosstalk characterization and correction algorithms using the lunar signal itself. Section 4 qualitatively and quantitatively assesses the improvements from the applied crosstalk correction. The improvements of the crosstalk correction are explained by the visual appeal of the images before and after correction; wherein the reduction in striping and removal of extraneous surface signal are highlighted from the Baja Peninsula images. Scenes with varying dynamic range are chosen in order to quantify the radiometric fidelity of the correction. The quantitative evaluation of the correction was assessed using three well-characterized sites Dome C, Pacific Ocean and Libya 1 [12] with scene ranges from about 0.5 typical radiance ($L_{typical}$) to about 1.1 $L_{typical}$. The long-term drifts in the retrieved Brightness Temperature (BT) from these sites are discussed, along with their reduction after the crosstalk correction is implemented. Finally, the summary section gives an in depth account of the band 28 crosstalk characterization, correction and mitigation.

2. PHENOMENA OF CROSSTALK EFFECT

The detector performance in band 28 has tended to be noisier since 2010 and consequently the direct impact can be seen in the visual quality of the EV L1B imagery. Also, the lunar images can be used to illustrate the crosstalk effect. In order to give a sense of the crosstalk direction, two sets of images of Baja California from 2001 and 2012 are analyzed. One of the unique features about the Baja peninsula is that the scene has a distinct ocean-to-land boundary that gives a clear visual quality comparison. Also, the same EV target was used in the analysis of band 27 which helped in identifying the extra ground target signal [7]. In addition to complement the EV images, two sets of lunar imagery around the same time frame were chosen.

Figures 2 and 3 are three dimensional surface creations of the integrated lunar observations for detector 3. The z-axis labels the magnitude of the lunar signal plus the background signal as observed from the sector rotated EV port [8]. The x-axis gives the along-scan direction (frames).Since the lunar size for each of the 1 km bands is about 7 × 7 pixels, the center 7 frames in the lunar images are the lunar signal of the band 28 detector 3 but the remaining frames will correspond to the signal in the neighboring bands. The y-axis gives the along-track direction (scans). Since there is an oversampling effect [8], there are several scans corresponding to one pixel in the along-track direction. Thus, there is an elongation effect in the lunar images shown in Figures 2 and 3. The oversampling factor is event-dependent and, thus, the elongation effect varies with event. In an ideal case only the background signal would exist in the neighboring frames, and it would correspond to the dark offset value of that band. Any additional response in the neighboring frames therefore corresponds to the crosstalk signal from the neighboring bands, which are called sending bands. Figures 2 and 3 show the lunar observations for band 28 detector 3 as acquired in 2000 and 2012 respectively. In each of the two figures, the portion of the signals shaped like a cylinder of magnitude 150 and above represents the moon surface. The neighboring hills and valleys located near the tall cylinders represent the crosstalk magnitude as observed in the two acquisitions. In general, the lunar signal has a typical response value of close to 4000 for the non-saturated band 31. In the case of other TEBs, such as band 28, a ratio of band 28 responses over band 31 is used to mimic the lunar response. Details on the ratio methodology have been discussed in reference [7]. However, in the two illustrations of the lunar surface, the magnitudes were significantly truncated in order to better illustrate the crosstalk signal. It is quite interesting to note that the crosstalk signal tended to have a positive magnitude early in the mission, indicating an addition of extraneous signal which is very similar in nature to the crosstalk in band 27 [7]. As time progressed, the crosstalk has changed its sign and has become fairly negative in magnitude again, keeping in trend with the crosstalk in band 27. This is very well complemented by analyzing the EV imagery qualitatively and quantitatively.

The EV imagery (as shown in Figures 4 & 7) plotted as BT for the Baja peninsula region, shows the detector-to-detector mismatch. Qualitatively from Figures 4 and 7, the striping intensity for various detectors is proportional to the crosstalk magnitude as observed in Figures 2 and 3.

Further, a line profile along the horizontal and vertical dotted lines (in the x and y direction) of the Baja peninsula in Figs. 4 and 7 are shown in Figures 6 (a & b) and Figures 9 (a & b), respectively, in order to give a quantitative sense of the crosstalk contamination. Figures 6a and 9a correspond to detector 2. Band 28 is a water vapor band. It should sense negligible ground surface. In the case of 2001 as shown in Figure 6a, there exist abrupt changes at pixess 700 and 837 indicating the ocean land boundaries. They amount to about 1.5 K drop from approximately 261.5 K and 2 K increase from 258.5. The same profile as shown in Figure 9a for 2012 image revealed similar drop and increase feature across the ocean land boundaries at pixels 556 to 694. The ocean-land edge feature at pixel 694 is not as clear as that at frame 556 and those shown in Figure 6a. This is because the scene BT itself decreases across the scan. From the along track profiles as shown in Figures 6b and 9b, the detector–to-detector differences are significantly different. The striping intensity has increased and changed with time. This observation along with the moon measurements have corroborated that the electronic crosstalk from bands 27, 29-30 have significantly impacted the response in band 28.

3. CROSSTALK CORRECTION ALGORITHMS AND COEFFICIENTS

This section will cover in depth the crosstalk characterization and correction algorithms based on the regularly scheduled moon observations through the SV port. The first subsection details the linear correction model which is adopted from the crosstalk characterization of band 27. In the next subsection, the characterization of the crosstalk coefficients from each of the three sending bands is explained.

3.1 CROSSTALK CORRECTION ALGORITHMS REVIEW

Electronic crosstalk is induced by the electromagnetic induction among the electric currents in electronic circuits of different bands on the same FPA. Since the bands on the FPA are located at different sites as seen in Figure 1, they view the same target at different times and consequently their electronic responses to the same target occur at different times. Then crosstalk of a sending band induces a ghosting image in the image of the receiving band, which is an intensity-reduced image of the sending band with geolocation shifted along the scan direction. The geolocation shift along the scan is measured by frame or pixel shift and the number of the frame shift equals the actual physical distance in the unit of the actual detector size from the sending band to the receiving band on the FPA. A receiving band can have several sending bands for multiple ghost images with different frame shifts, which are superimposed with the real image. The electronic crosstalk may change with on-orbit deterioration of the circuits but should not change with the degradation of the relevant detectors, the optical elements or the spectral changes of the detectors. Since the electronic crosstalk is electromagnetic induction effect, its contribution to the signal of the receiving band can be positive as well as negative. The contribution can also change from positive to negative or vice versa depending on the change of the electric circuits in the

FPA. Besides the electronic crosstalk, there can also be optical crosstalk, which is also called optical leaks. The optical crosstalk of a detector in a band is mainly induced by the imperfection of the detector's filter or other mechanisms related to optical transmittance or paths. It does not induce a ghost image with frame shifted. Since electronic crosstalk signal of a sending band has a frame shift from the real signal and the optical leak signal, its effect can be separated given certain conditions such as the viewing of a point-like target like the Moon. In this analysis, we focus on the analysis of the electronic crosstalk effect.

The electronic crosstalk correction algorithm is based on a simple linear model with the effective crosstalk coefficient calculated as a band-averaged estimate from the sending band and characterized for each detector on the receiving band. The algorithm is the same as one applied to the band 27 crosstalk correction algorithm detailed in [7]. Following provides the correction equation

$$dn_{B_rD_r}(F) = d^{msr}_{B_rD_r}(F) - \sum_{B_s} C(B_r, D_r, B_s)\left\langle dn^{msr}_{B_sDs}(F + \Delta F_{rs})\right\rangle_{D_s}, \quad (1)$$

where dn is the background subtracted instrument response, B, D refer to band and detector, r and s correspond to the receiving and sending bands, *msr* indicates that the dn is measured instrument response with crosstalk correction, $C(B_r,D_r,B_s)$ is the sending band averaged crosstalk coefficient for the crosstalk from band B_s to band B_r detector D_r, F is the frame number along the scan, and F_{rs} is frame shift between bands B_s and B_r. The crosstalk coefficients can be derived from the lunar observations since the Moon is a point-like light source even though it has a finite size. The basic idea is that neighboring hills and valleys located near the central tall cylinder signal in a lunar image are induced by the crosstalk. The coefficients can then be determined using Eq. (1) by forcing the left side of the equation to be zero. Since there is no frame shift in the signal of a potential optical leak, it should have no impact in the derived crosstalk coefficients from the lunar observations. Thus, the derived crosstalk coefficients are mainly for the electronic crosstalk. Eq. (1) is required to be applied to correct the dn for both the BB and EV. In other words, it should be applied to BB calibration to correct the crosstalk effect in calibration coefficients and in L1B code with new crosstalk effect corrected calibration coefficients to remove the crosstalk contamination in EV radiance and then in brightness temperature units.

3.2 CROSSTALK CORRECTION COEFFICIENTS

As mentioned earlier, MODIS views the lunar surface approximately monthly. This allows a fairly exhaustive characterization of the crosstalk coefficients temporally. Figures 10-12 show the crosstalk coefficient magnitude for band 28 from each of the previously mentioned sending bands. The coefficients are derived from the lunar observations with the approach briefed in

Section 3.1 and detailed in [7]. For each of the plots, the crosstalk coefficients for most detectors start out to be slightly positive early in the mission. The crosstalk coefficient for band 28 detector 2 is the first among other detectors that change in direction and magnitude over the lifetime. The coefficient for this detector drops to about -0.015 for sending band 27, by about -0.058 for sending band 29 (8.55 μm), and by about -0.016 for sending band 30 (9.73 μm) in 2001 and remains fairly constant at those levels over time. As an example, another detector no. 3 shows a steady and gradual change in crosstalk coefficient magnitude and direction. The coefficient for detector 3 is positive in nature for sending band 27 until 2002 after which there is a slow drift to about -0.01 over the entire mission time. A similar trend is observed for sending band 29 with the only difference being the rate of drift is quite fast in comparison to the sending band 27. The crosstalk coefficient reached to about -0.05 by 2013. The crosstalk coefficient from sending band 30 is quite similar in nature to band 27 and is currently about -0.015. Detectors 8 and 10 are interesting examples for sudden large drops in terms of coefficient trends. The drops occurred in all the sending bands around mid 2004 and mid 2005 respectively. The abrupt switch from the positive to negative direction needs careful treatment while characterizing the crosstalk magnitude. To reduce the overall small fluctuations induced due to the seasonality and other effects, and to allow a more robust characterization of crosstalk correction coefficients used in the L1B correction, the coefficients are averaged over a period of every 6 months. In the event of a sudden change, the moving average of the actual jerk point is used in order to reflect the real change in the trending. All the above mentioned changes are consistent with the NEdT trends for each of the detectors in band 28. Also, these detectors have been identified as ‘noisy’ based on performance and classified as same in the official quality assurance (QA) LUT in L1B products. In the case of the less noisy detectors, the crosstalk coefficients have tended to gradually drift from the positive to negative direction. A typical example of nominally operating detector is detector 5 which has the smallest magnitude of crosstalk over the entire lifetime. This is the only band 28 detector whose crosstalk coefficients tend to be very stable and remain positive in magnitude throughout the lifetime of the instrument.

The crosstalk pattern changes and becomes more serious with time as demonstrated in Figures 10-12. As mentioned previously, this is mainly due to the deterioration of the electronic circuits of the relevant bands in the LWIR FPA. With the crosstalk coefficients derived, it is necessary to assess if the characterization is sufficient and crosstalk pattern changes with time as demonstrated by the crosstalk coefficients. Hence the crosstalk correction is applied to band 28. The improvements are highlighted in detail in the next section which would cover the removal of extraneous features in the EV imagery as well as the balance of the radiometric gain of various detectors of band 28. This would validate the effectiveness of crosstalk coefficients and the characterization approach used.

4. CROSSTALK CORECTION

Three important aspects are covered in this section. First, the improvements are assessed by applying them to the dominant calibration term (BB based gain) and also the application to the EV dn response. Next, a qualitative and quantitative assessment is done on the Baja Peninsula ground target as discussed in Section 2. Finally, a complete evaluation of the radiometric improvements with the electronic crosstalk correction is performed and the results are presented.

4.1 CROSSTALK CORRECTION FOR CALIBRATION COEFFICIENTS

The MODIS TEB calibration algorithm is well documented and explained in several references [9]-[11]. In the context of the work presented, only a brief description is provided for the TEB calibration. A quadratic model is used to establish a relationship between the 'at' sensor aperture radiance as viewed from the on-board BB and the instrument response as measured by each individual detector. The linear term in the quadratic model is referred to as the b_1 term whose inverse gives the gain of the TEBs. Since the detectors in the TEB view the BB every scan, the same is applicable for the calculation of b_1. The non-linear and the offset terms are significantly smaller quantities in comparison to b_1 and have minor impact on the calibration. Therefore, in this paper we delve into the impact of crosstalk correction on the linear calibration term. Figure 13 gives the b_1 coefficient trend over lifetime and is sampled roughly 60 days. Each point is a granule-averaged estimate computed over approximately 101 scans per each mirror side [6]. From Figure 14, it can be noticed that the b_1 coefficients of detectors 2, 3, 8, 9, and 10 have sudden jumps that cause abrupt discontinuities in the long-term trend. As mentioned in the earlier sections, these correlate with the noisy behavior indicated by the NEdT trends. Figure 14 shows the b_1 trend after the crosstalk correction is applied. It is quite clear from these trends that afore mentioned jumps in b_1 are significantly reduced and the long-term trend shows a slow drift, which is expected in the case of normally operating detectors devoid of crosstalk. Also, after the correction, the b_1 response between detectors is tighter indicating that the detector-to-detector differences are also small. A direct impact of this in the EV imagery would show a reduction in the striping artifacts as seen in Figures 5 and 8. The maximum band-averaged b_1 change after the crosstalk correction for band 28 is approximately 6.5%. This amounts to approximately a 2 K change after correction at the typical radiance levels ($L_{typical}$). Since crosstalk is impacted both in EV and BB responses, the amount of change in terms of BT can be as large as 4.5 K at $L_{typical,}$ and this is well illustrated in the next subsection.

4.2 CROSSTALK CORRECTION IN L1B PRODUCTS

The crosstalk correction was applied to the Baja peninsula test scenes shown in the earlier sections. Early in the mission, Terra band 28 exhibited noisy behavior mainly for detector 2, and hence the striping artifact is caused due to the radiometric imbalance of this detector. After the crosstalk correction is applied to the Baja Peninsula image from 2001 that shows Figure 5, the striping artifact is significantly decreased. A qualitative look into the 2012 image as shown by Figure 8 indicates a radiometric balance in the response of the aforementioned noisy detectors.

The profiles along the horizontal and vertical dotted lines in Figs. 5 and 8 are displayed in Figs. 6 and 9, respectively.

Figure 6a also gives the horizontal profile of the scene from 2001 after correction and is emphasized by the solid line. The horizontal profile shows sharp edges and faint resemblance of the Baja peninsula feature content i.e. sea surface and land boundaries before and after correction, respectively. Based on the horizontal profile (detector 2 as example) before and after correction there is a reduction of this feature content by approximately 2 K. The same Baja Peninsula region when examined in 2012 also shows a significant reduction of the sea land boundary feature by about same amount as in 2001 scene before and after correction, and is illustrated via Figure 9a. Therefore, in the horizontal direction the ground feature contamination for detector 2 in 2001 was approximately 2 K and has kept the same amount to 2012. This is consistent with the detector's crosstalk coefficients shown in Figs. 10-12. The crosstalk coefficients of the detector for all the three sending bands had sudden changes in 2000 and have kept almost constants since then. For other detectors such as detector 8, the ground feather contamination changes with time since their crosstalk coefficients change with time as demonstrated in Figs 10-12. In order to assess the improvements in striping the vertical profile before and after the correction are studied carefully, illustrated by Figures 6b and 9b. Again solid lines indicate the profile after the correction. The detector-to-detector differences in 2001 are in the range of about 5 K before the correction and are significantly reduced to within 1 K after the crosstalk correction is applied. Similar range of correction is observed in the 2012 Baja Image. However, the number of pinks in the profile of 2012 is tripled compared to that of 2001, demonstrating the crosstalk contamination becomes pronounced in the later years that have been dealt with in the previous sections. Overall, from both the horizontal and vertical profiles it is quite evident that the crosstalk coefficients and its correction work well. In order to get a complete handle on the improvements seen by crosstalk correction the effects were assessed using three well-characterized sites at varying radiance levels. Dome Concordia (Dome C), Libya and the Pacific Ocean were the three sites chosen. These sites have proven to be good radiometric test sites from the analysis reported in [12].

The Dome C site is one of the several summits of the Antarctica ice sheet and considered as the most homogeneous Earth target by the Concordia research stations jointly operated by France and Italy. With this site well understood, both vicariously and through cross sensor comparisons [13] allow a unique vantage point in assessing long-term instrument related drifts and changes. The scene radiance levels are below the 0.3 $L_{typical}$ for MODIS TEBs and hence an ideal test location for assessing at the low end of the dynamic range. Also, the site being at the south pole of the Earth, most remote sensing satellites such as MODIS have a unique advantage of making several overpasses in any given day. Thus, in the MODIS L1B archive exist several high quality data acquired over the Dome C region. As mentioned at the beginning, MODIS being a wide angle viewing spectroradiometer, the MODIS data in any given scan has response versus scan angle (RVS) dependencies [14]. Thus, in order to negate these impacts in the current study, only

those scenes with nadir viewing angles were considered. This amounted to over 1500 EV acquisitions covering about 14 years of satellite lifetime data. For all the test scenes in this work only the latest collection (C6) of the MODIS L1B radiances are used. Next, the data were processed as follows. For each scene the BT was computed using the Planck equation over a small region of 40 × 40 MODIS area with the center pixel corresponding to the center latitude and longitude of Dome C. The BT for each detector was averaged over the corresponding pixels in this sub region before and after the crosstalk correction. The same processing strategy is adopted in the other test sites as well. Figure 15 shows the long term trend of the retrieved MODIS Terra band 28 C6 BT since epoch 2000 over the selected region. The trend shows a seasonal oscillation for all the detectors with the minimum retrieved BT of approximately 205 K and a maximum retrieved BT of approximately 240 K. Figure 16 presents the detector-to-detector difference with respect to the band average before the crosstalk correction. Based on the plot, it can be seen that the difference for most detectors is about ±0.8 K. The BT of detector 8 is about 1 K lower than the band-averaged value since 2004. Similarly, the BT of detector 2 is about 0.5 K lower than the band average since 2001. This corroborates the striping noise seen in images over the Dome C site, which is consistent with the results shown in previous studies as mentioned in [15]. Next, the actual amount of the crosstalk correction induced in each of the detectors is shown in Figure 17. The amount of correction in general for various detectors roughly varies from about -0.5 K in early life to as high as 2 K in 2010 and then settling at about 1.5 K by late 2012. The band average of the detector-dependent crosstalk correction is also shown in Figure 17 through the heavy solid line, which shows a correction amount of about -0.3 K in the beginning of the mission to 0.4 K by late 2012. This amounts to a total band-averaged correction of roughly 0.7 K over the entire mission. This crosstalk correction amount is very close to the long-term bias as seen from the Terra and Aqua MODIS relative bias comparisons over the Dome C site as reported in [15]. Figure 18 presents the detector-to-detector difference after the crosstalk correction is applied. The detector differences in general are within ±0.65 K throughout the mission time. This shows that, after the crosstalk correction, there is some residual effect, which is not accounted for but within uncertainty of 1% in radiance. Finally, Figure 19 shows the Terra band 28 band-averaged BT long-term trend before and after the crosstalk correction. The BT curve before the crosstalk correction shows almost a change from about 220.7 K to about 221.5K over the lifetime. The trend for the BT after the crosstalk correction indicates a fairly linear change over time from about 220.6 K to about 222 K over the mission. As mentioned in Section 4.1 that the gain of the instrument after the crosstalk correction will induce about 2 K change in the retrieval. Therefore, it is conceivable that the trend observed is keeping track with the overall instrument change. However, the Dome C site is well below the $L_{typical}$ and hence other effects in the overall calibration will not be considered here but subject to future examination

The Pacific Ocean site is also a well-understood site as an EV target and generally provides radiance close to the typical temperatures for most MODIS TEBs including band 28. The

analysis was performed in similar fashion to the Dome C site with an additional condition of using scenes acquired with a repeat cycle of every 16 days. This observation frequency guarantees that the same geo location and view geometry is used. Figure 20 shows the lifetime Terra band 28 C6 BT trend of the Pacific Ocean site for each detector. There is a seasonal variation from about 255 K to 271 K over the 14 years of Terra MODIS acquisitions for this band. Next, the detector-to-detector differences before the crosstalk correction are shown in Figure 21. Detectors 1, 4-7, and 10 have positive differences from the band average by about 1 K while detectors 2-3, and 8-9 have negative differences of approximately 1.8 K. Also, as shown previously, the latter detectors are all noisy in nature and are significantly contaminated by crosstalk. The magnitude of the crosstalk correction for all the detectors is shown in Figure 22. Figure 22 is very much in correlation with the inferences drawn from Figure 21. The detectors with positive differences for the band average tend to have the crosstalk correction magnitude vary from about -1 K to 0.4 K over the lifetime. In comparison the other set of detectors (i.e., ones with negative differences for band average) showed the magnitude of the crosstalk correction to be varying from about -0.6 K to about 2.5 K with a maximum change of approximately 3 K for detector 8. This is anticipated as the crosstalk coefficients for these detectors exhibited such a change (refer to Figures 10-12). The band-averaged correction amount is also shown through the heavy solid line in Figure 22. The average correction has varied from about -0.5 K in early life to about 1.1 K in late 2012 data. The actual amount of average correction change from 2000 to 2012 is about 1.6 K at typical temperatures for band 28. After correction, the detector-to-detector differences for all detectors are essentially flat and well within ± 0.6 K as shown Figure 23. Finally, the long-term drifts in band 28 BT before and after the crosstalk correction is assessed and presented in Figure 24. The long-term drift before the crosstalk correction is provided by the solid curve and is assessed to be about 2.7°K drop in a non-linear fashion. After the crosstalk correction the long-term drift is found to be significantly reduced and is about 1.1 K change in slow fashion. In general, this slow drift in air temperature over sea surfaces is expected and has been observed through various climatic studies [17]. This shows that the crosstalk correction definitively corrects the radiometric output and also matches the actual expectation of the scientific geophysical parameter over the ocean surface. Therefore, at $L_{typical}$ levels the crosstalk correction accounts for approximately the expected amount of change.

The Libya 1 desert site is considered as a radiometric super site, is highly recommended and is exceedingly good pseudo invariant target which can be used for inter satellite comparisons by the Committee of Earth Observation Satellites [14], [18]. The Libya 1 site has also been found very useful for deriving calibration terms such as RVS for the MODIS RSBs [16]. Since this area is sparse and arid, the water vapor channel should contain minimal fluctuations in the retrieved BT, with the fluctuations mainly due to diurnal changes. Once again, similar treatment was done in the data selection and processing as in the case of the Pacific Ocean site. The lifetime BT trend for band 28 over the Libya 1 site is given by Figure 25. The BT levels on average are greater

than 1.2 $L_{typical}$. The long-term trend shows an oscillation of the BT levels from approximately 258 K to 275 K. The detector-to-detector differences are presented in Figure 26. Over a period of 14 years, the BT differences for various detectors have significantly changed. The differences for the earlier mentioned noisy detectors are as high as -4 K and some of the nominally operating detectors such as detector 5 have differences as high as 2 K. The magnitude of the crosstalk correction in terms of BT for the various detectors is shown in Figure 27. A correction magnitude of 5 K is observed for detector 8 from 2008 to late life. In contrast, detector 2 has a fairly constant correction amount of about 2.5 K over the lifetime. Most of the nominally operating detectors have a crosstalk correction amount of approximately 1 K over the mission time. Figure 27 also shows the band average crosstalk correction with the heavy solid curve. On a band-averaged level the correction amount is about 1.7 K over the lifetime. Next, the detector-to-detector difference after correction is examined and is provided by Figure 28. After the crosstalk correction is applied, the detector differences are reduced to be within ±0.65 K. This would significantly help in removing striping noise from the Libya 1 scenes. Figure 29 presents the Terra band 28 BT trend before and after the crosstalk correction. The results of the crosstalk correction from the Libya 1 desert site show that the long-term drift in the retrieved BT is approximately -1.2 K over 14 years of operation. The actual drift before correction is observed to be about -2.9 K for the same period. A typical desert site such as Libya 1 is dry with very little variation in the air temperature during the day, with the exception of the precipitation periods and a relatively cooler and stable air temperature during night. This essentially means that, barring the drastic seasonal variations as expected in arid regions, the long-term drift should be minimal. The crosstalk correction thus significantly decreases this long-term drift and in the process restores the true variability of the region.

5. SUMMARY

The paper presents a thorough investigation of Terra MODIS band 28 electronic crosstalk. A linear characterization model has been developed similar to that for Terra MODIS band 27. The sending bands were identified to be the neighboring bands 27, 29 and 30 on the same LWIR FPA. With the crosstalk characterization achieved from the regular lunar observations of MODIS, a correction was implemented on two fronts. First, the on board BB which is used for the calibration of TEB was corrected for the band 28 response. Next, the correction was implemented on EV scenes. The Baja peninsula images were shown before and after the crosstalk correction. The corrected images showed significant reduction in striping artifacts and radiometrically balanced response between various detectors. Also, the weak ghosting features observed on the land sea boundaries were reduced significantly. Further, the corrections were applied on three well-characterized sites to assess the radiometric improvements over the wide dynamic range. From the Dome C site, the lifetime BT trends essentially showed a linear change over time by about 1.4 K after the crosstalk correction was applied. The detector differences were significantly reduced over the lifetime and were found to be within ± 0.75 K. At typical levels, the crosstalk correction on the Pacific Ocean site confirmed the previously observed drifts

as in the Baja Peninsula test cases. The maximum amount of the crosstalk correction was observed on the Libya 1 desert site. Based on the radiometric correction amounts, it is clear that the amount of correction is dependent on the signal levels. It is noted that the crosstalk is continuing to show its severity in the later years, particularly since mid-2010, and is expected to become larger with time. Therefore, a very good characterization and correction of the electronic crosstalk in band 28 is imperative to ensure the radiometric quality of the L1B products. At close to typical and higher radiance levels, i.e., the Pacific Ocean and Libya 1 sites, we showed that the crosstalk correction could reduce the detector differences to within ±0.6 K, The crosstalk correction algorithm thus substantially improves both the image quality and radiometric accuracy of the Terra band 28 L1B products.

ACKNOWLEDGEMENTS

The authors would like to thank Dr. Brij Gambhir and Dr. Mike Chu for their helpful comments and suggestions. The views, opinions, and findings contained in this paper are those of the authors and should not be construed as an official NOAA or U.S. Government position, policy, or decision.

REFERENCES

[1] V. V. Salomonson, Barnes, W. L., Xiong, X., Kempler, S., and Masuoka, E., "An Overview of the Earth Observing System MODIS Instrument and Associated Data Systems Performance", *Proc. IGARSS* 2, 1174-1176 (2002).

[2] W. L. Barnes, Xiong, X., and Salomonson, V. V., "Status of Terra MODIS and Aqua MODIS", *Proc. IGARSS* 2, 970-972, 2002.

[3] C. L. Parkinson, "Aqua: An Earth-Observing Satellite Mission to Examine Water and Other Climate Variables", *IEEE Trans. Geosci. Remote Sens.* 41, 173-183 (2003).

[4] B. Guenther, W. Barnes, E. Knight, J. Barker, J. Harnden, R. Weber, M. Roberto, G. Godden, H. Montgomery, and P. Abel, "MODIS Calibration: A Brief Review of the Strategy for the At-Launch Calibration Approach", *J. Atmos. Oceanic Technol.* 1, 274-285, 1996.

[5] X. Xiong, K. Chiang, A. Wu, W. Barnes, B. Guenther, and V. Salomonson, "Multiyear On-orbit Calibration and Performance of Terra MODIS Thermal Emissive Bands", *IEEE Trans. Geosci. Remote Sens.* 46, 1790-1803, 2008.

[6] X. Xiong, B. Wenny, A. Wu, and W. Barnes, "MODIS On-board Blackbody Function and Performance", *IEEE Trans. Geosci. Remote Sens*. 47, 4210-4222, 2009.

[7] J. Sun, X. Xiong, S. Madhavan, and B. N. Wenny, "Terra MODIS Band 27 Electronic Crosstalk Effect and Its Removal", *IEEE Trans. Geosci. Remote Sens.* 52, 1551-1561, 2014.

[8] J. Sun, X. Xiong, W. Barnes, and B. Guenther, "MODIS Reflective Solar Bands On-Orbit Lunar Calibration", *IEEE Trans. Geosci. Remote Sens.* 45, 2383-2393, 2007.

[9] X. Xiong, K. Chiang, J. Esposito, B. Guenther, and W. L. Barnes, "MODIS on-orbit calibration and characterization," *Metrologia* 40, 89–92, 2003.

[10] X. Xiong, K. Chiang, B. Guenther, and W. L. Barnes, "MODIS thermal emissive bands calibration algorithm and on-orbit performance," *Proc. SPIE* 4891, 392–401, 2002

[11] X. Xiong and W. L. Barnes, "An overview of MODIS radiometric calibration and characterization," *Adv. Atmos. Sci.*, 23, 69–79, 2006.

[12] J. Sun, X. Xiong, Y. Li, S. Madhavan, A. Wu, and B. N. Wenny, "Evaluation of Radiometric Improvements With Electronic Crosstalk Correction for Terra MODIS Band 27", *IEEE Trans. Geosci. Remote Sens*. 52, 6497-6507, 2014.

[13] B. N. Wenny and X. Xiong, "Using a cold earth surface target to characterize long-term stability of the MODIS thermal emissive bands," *IEEE Geosci. Remote Sens. Lett.* 5, 162–165, 2008.

[14] J. Sun, X. Xiong, A. Angal, H. Chen, X. Geng, and A.Wu, "On-orbit performance of the MODIS reflective solar bands time-dependent response versus scan angle algorithm," *Proc. SPIE* 8510, 85100J, 2012

[15] B. N. Wenny, X. Xiong, and S. Madhavan, "Evaluation of Terra and Aqua MODIS thermal emissive band calibration consistency," *Proc.SPIE* 8533, 853317-1–853317-9, 2012.

[16] J. Sun, X. Xiong, A. Angal, H. Chen, A. Wu, and X. Geng, "Timedependent response versus scan angle for MODIS reflective solar bands," *IEEE Trans. Geosci. Remote Sens.* 52, 3159-3174, 2014.

[17] S. A. Morain and A. M. Budge, "Post-Launch Calibration of Satellite 660 Sensors," Proc. of the International Workshop on Radiometric and Geometric Calibration, December 2003, Mississippi, USA. NewYork, NY, USA: Taylor & Francis, Aug. 5, 2004, pp. 25–26.

[18] H. Cosnefroy, M. Leroy, and X. Briottet, "Selection and characterization of Saharan and Arabian Desert sites for the calibration of optical satellite sensors," *Remote Sens. Environ.* 58, 101–114, 1996.

Figure Caption:

Figure 1, MODIS LWIR focal plane.

Figure 2, Lunar response of Terra band 28 detector 3 in 2000.

Figure 3, Lunar response of Terra band 28 detector 3 in 2012.

Figure 4, Image of Terra band 28 temperature at Baja peninsula in 2001 (Before Correction). The temperatures along the horizontal and vertical dotted lines are displayed in Figures 6a and 6b, respectively.

Figure 5, Image of Terra band 28 temperature at Baja peninsula in 2001 (After Correction). The temperatures along the horizontal and vertical dotted lines are displayed in Figures 6a and 6b, respectively.

Figure 6a, Terra band 28 temperature along scan direction indicated by the horizontal dotted line in Figures 4 and 5 (2001190; dotted: before correction; solid: after correction). The two vertical dashed lines indicate the land-ocean edges.

Figure 6b, Terra band 28 temperature along track direction indicated by the vertical dotted lines in Figures 4 and 5 (2001190; dotted: before correction; solid: after correction).

Figure 7, Image of Terra band 28 temperature at Baja peninsula in 2012 (Before Correction). The temperatures along the horizontal and vertical dotted lines are displayed in Figures 9a and 9b, respectively.

Figure 8, Image of Terra band 28 temperature at Baja peninsula in 2012 (After Correction). The temperatures along the horizontal and vertical dotted lines are displayed in Figures 9a and 9b, respectively.

Figure 9a, Terra band 28 temperature along scan direction indicated by the horizontal dotted line in Figures 7 and 8 (2012198; dotted: before correction; solid: after correction). The two vertical dashed lines indicate the land-ocean edges.

Figure 9b, Terra band 28 temperature along track direction indicated by the vertical dotted lines in Figures 7 and 8 (2012198; dotted: before correction; solid: after correction).

Figure 10, Terra band 28 crosstalk coefficients for sending band 27.

Figure 11, Terra band 28 crosstalk coefficients for sending band 29.

Figure 12, Terra band 28 crosstalk coefficients for sending band 30.

Figure 13, Terra band 28 b1 before correction for individual detectors.

Figure 14, Terra band 28 b1 after correction for individual detectors.

Figure 15, Terra MODIS band 28 C6 brightness temperature at DOME C.

Figure 16, Terra MODIS band 28 C6 brightness temperature detector difference at DOME C.

Figure 17, Crosstalk correction for Terra MODIS band 28 C6 brightness temperature at DOME C.

Figure 18, Terra MODIS band 28 C6 brightness temperature detector difference at DOME C after crosstalk correction.

Figure 19, Dome C band averaged BT before (solid) and after (dotted) crosstalk correction.

Figure 20, Terra MODIS band 28 C6 brightness temperature at Pacific Ocean.

Figure 21, Terra MODIS band 28 C6 brightness temperature detector difference at Pacific Ocean.

Figure 22, Crosstalk correction for Terra MODIS band 28 C6 brightness temperature at Pacific Ocean.

Figure 23, Terra MODIS band 28 C6 brightness temperature detector difference at Pacific Ocean after crosstalk correction.

Figure 24, Pacific Ocean band averaged BT before (solid) and after (dotted) crosstalk correction.

Figure 25, Terra MODIS band 28 C6 brightness temperature at Libya 1.

Figure 26, Terra MODIS band 28 C6 brightness temperature detector difference at Libya 1.

Figure 27, Crosstalk correction for Terra MODIS band 28 C6 brightness temperature at Libya 1.

Figure 28, Terra MODIS band 28 C6 brightness temperature detector difference at Libya 1 after crosstalk correction.

Figure 29, Libya 1 band averaged BT before (solid) and after (dotted) crosstalk correction.

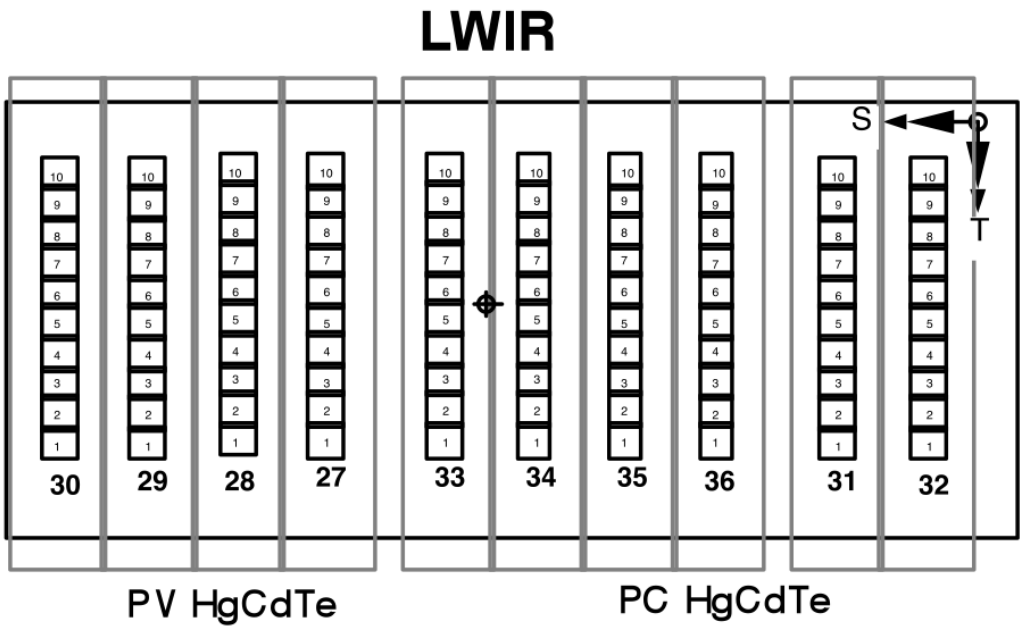

Figure 1, MODIS LWIR focal plane.

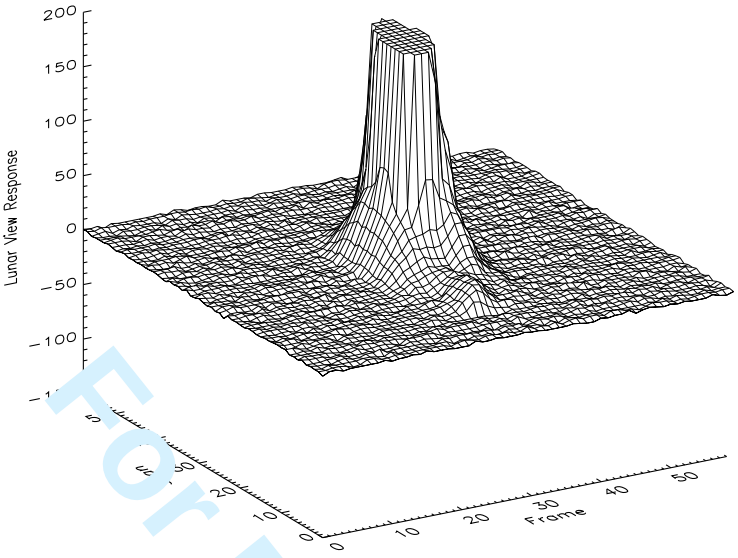

Figure 2, Lunar response of Terra band 28 detector 3 in 2000.

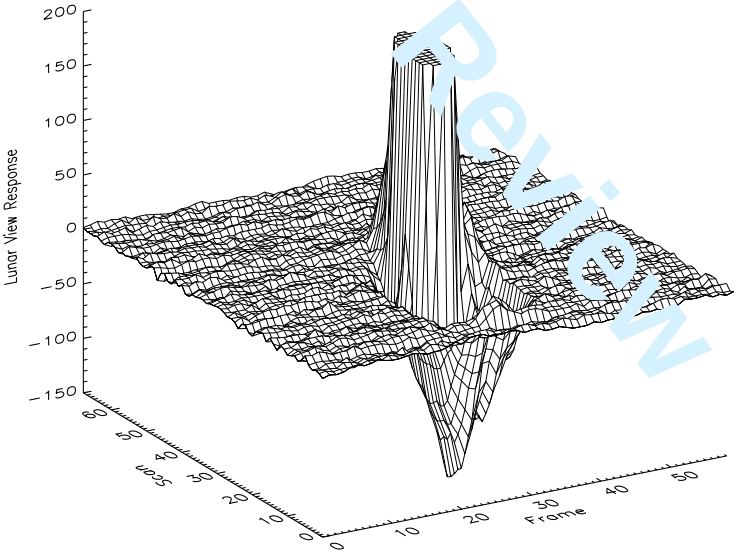

Figure 3, Lunar response of Terra band 28 detector 3 in 2012.

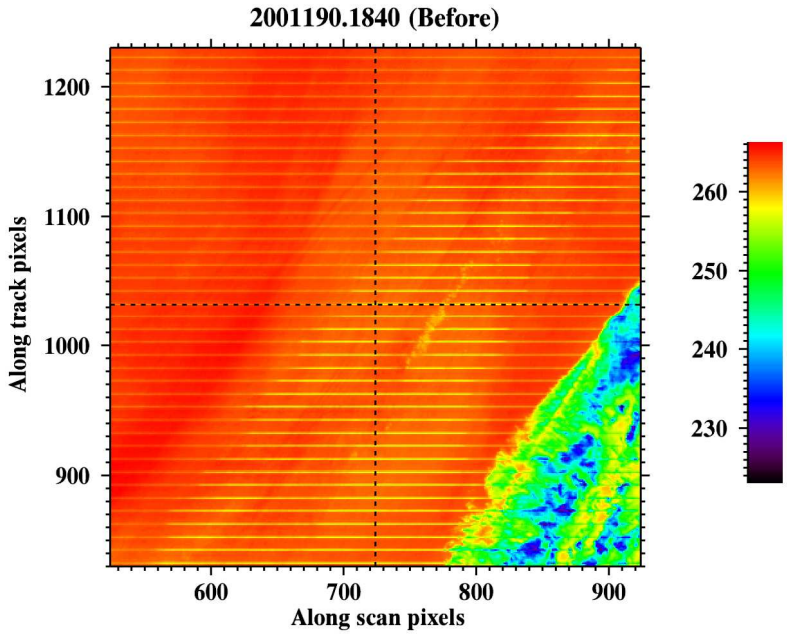

Figure 4, Image of Terra band 28 temperature at Baja peninsula in 2001 (Before Correction). The temperatures along the horizontal and vertical dotted lines are displayed in Figures 6a and 6b, respectively.

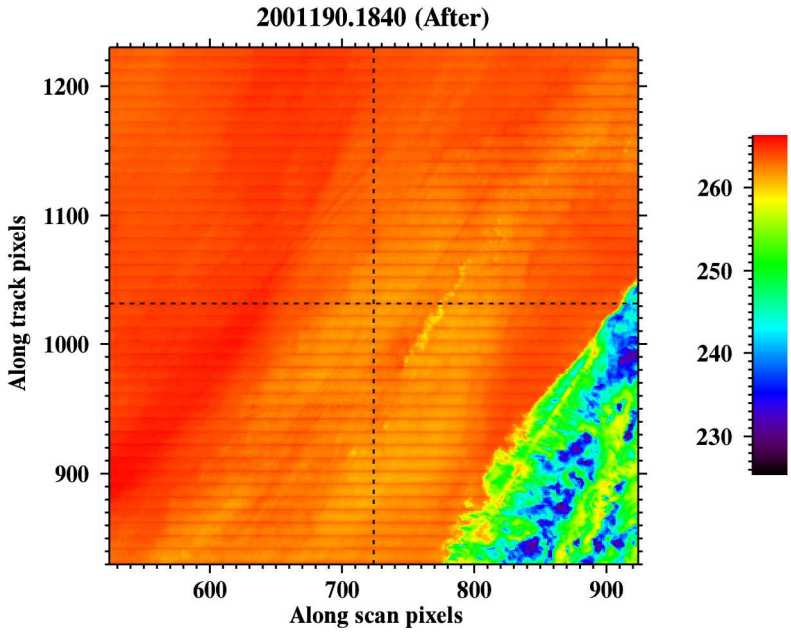

Figure 5, Image of Terra band 28 temperature at Baja peninsula in 2001 (After Correction). The temperatures along the horizontal and vertical dotted lines are displayed in Figures 6a and 6b, respectively.

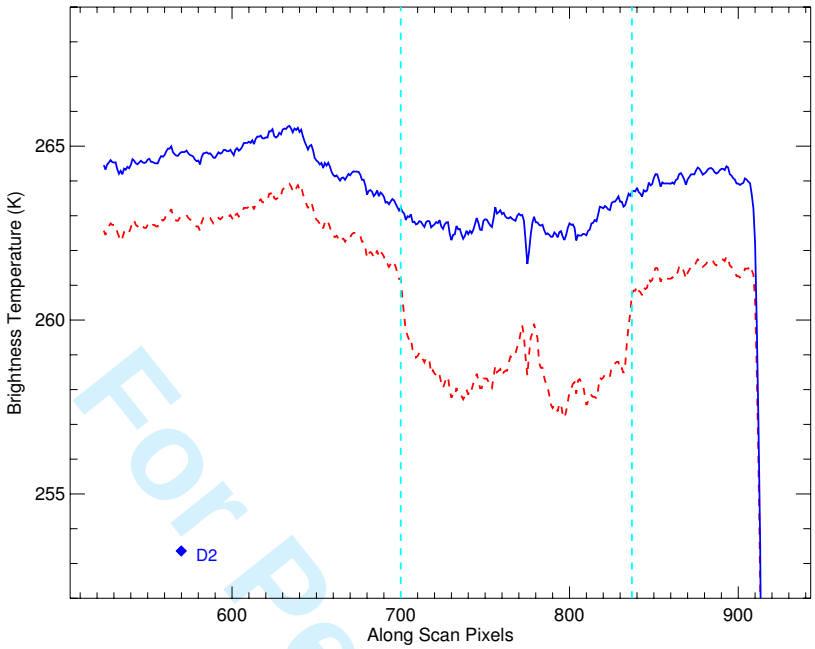

Figure 6a, Terra band 28 temperature along scan direction indicated by the horizontal dotted line in Figures 4 and 5 (2001190; dotted: before correction; solid: after correction). The two vertical dashed lines indicate the land-ocean edges.

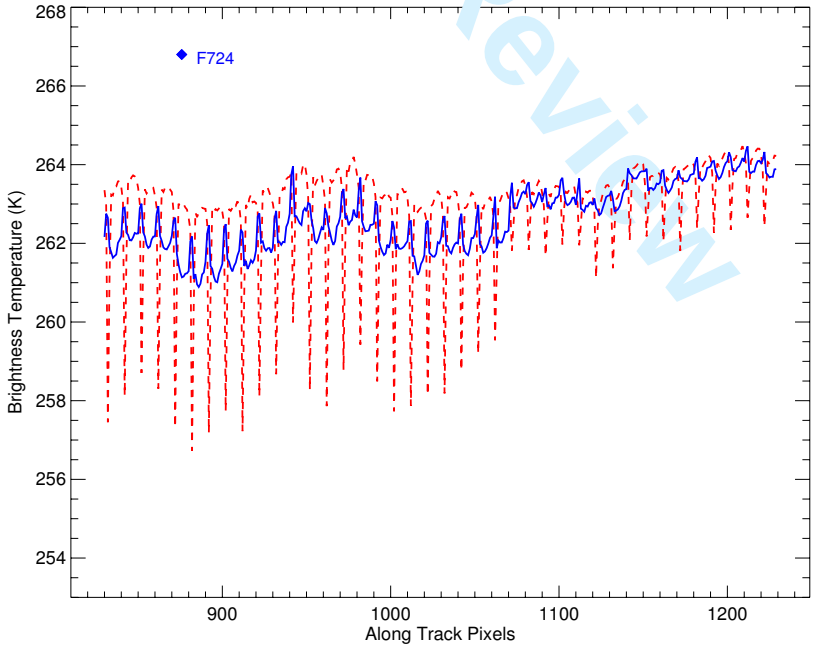

Figure 6b, Terra band 28 temperature along track direction indicated by the vertical dotted lines in Figures 4 and 5 (2001190; dotted: before correction; solid: after correction).

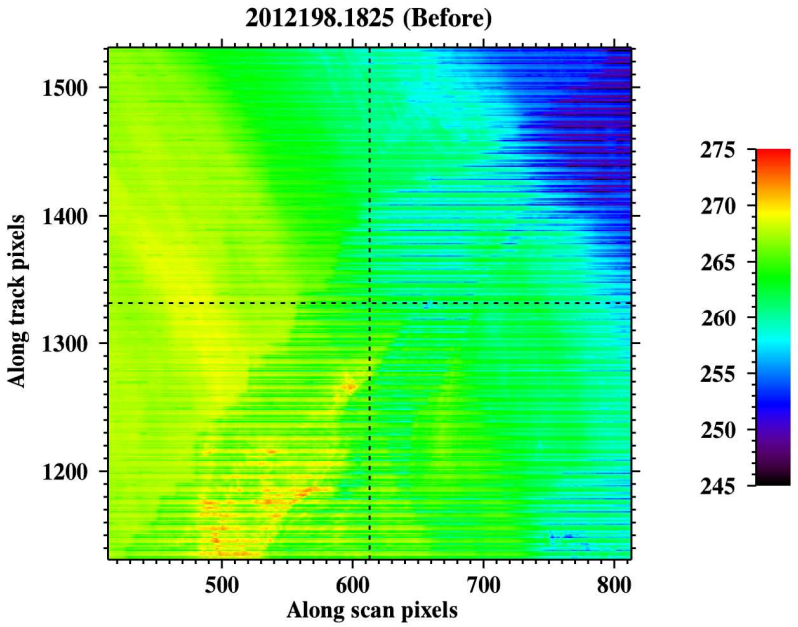

Figure 7, Image of Terra band 28 temperature at Baja peninsula in 2012 (Before Correction). The temperatures along the horizontal and vertical dotted lines are displayed in Figures 9a and 9b, respectively.

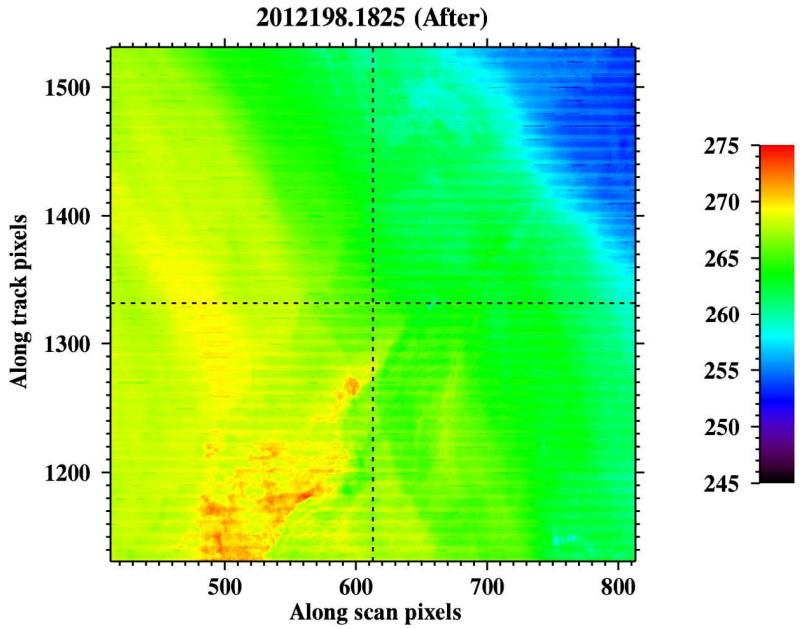

Figure 8, Image of Terra band 28 temperature at Baja peninsula in 2012 (After Correction). The temperatures along the horizontal and vertical dotted lines are displayed in Figures 9a and 9b, respectively.

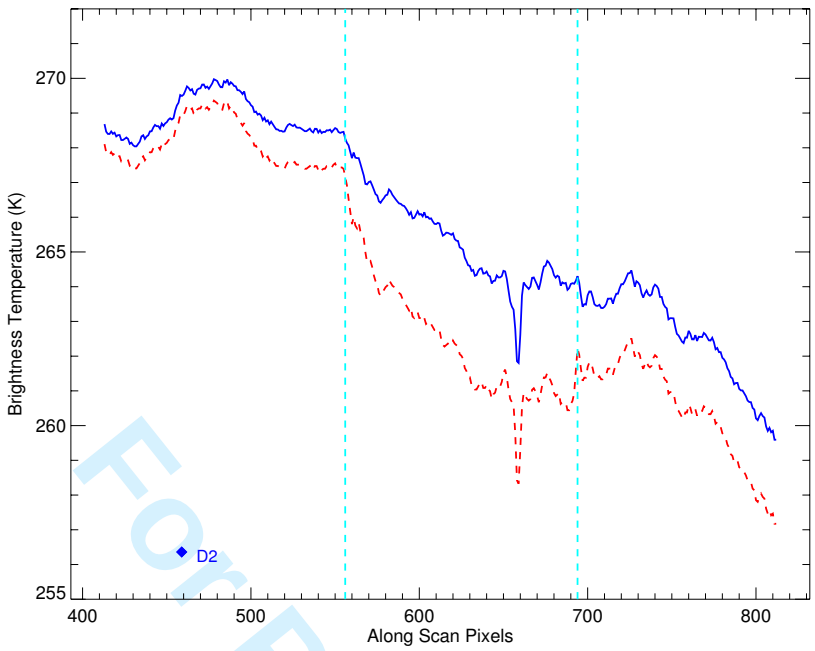

Figure 9a, Terra band 28 temperature along scan direction indicated by the horizontal dotted line in Figures 7 and 8 (2012198; dotted: before correction; solid: after correction). The two vertical dashed lines indicate the land-ocean edges.

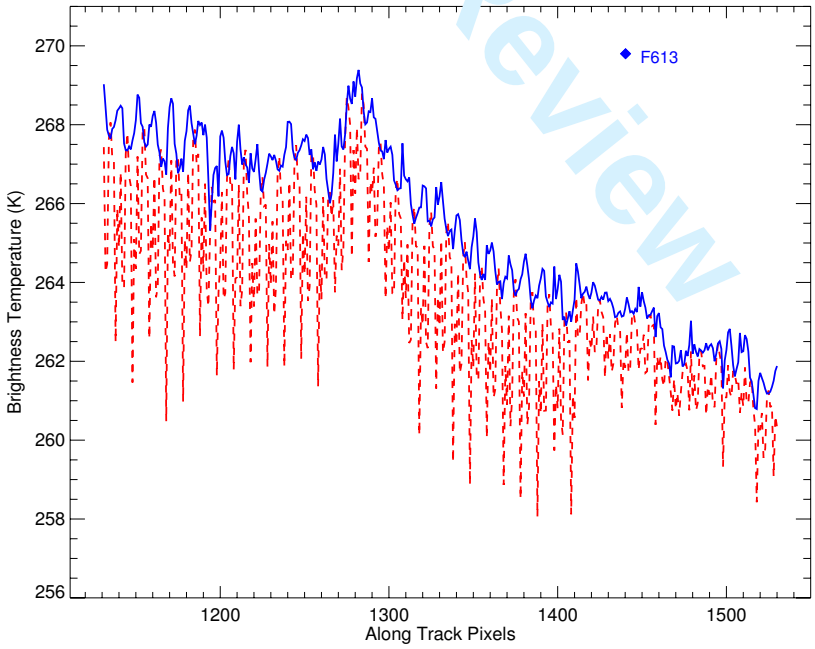

Figure 9b, Terra band 28 temperature along track direction indicated by the vertical dotted lines in Figures 7 and 8 (2012198; dotted: before correction; solid: after correction).

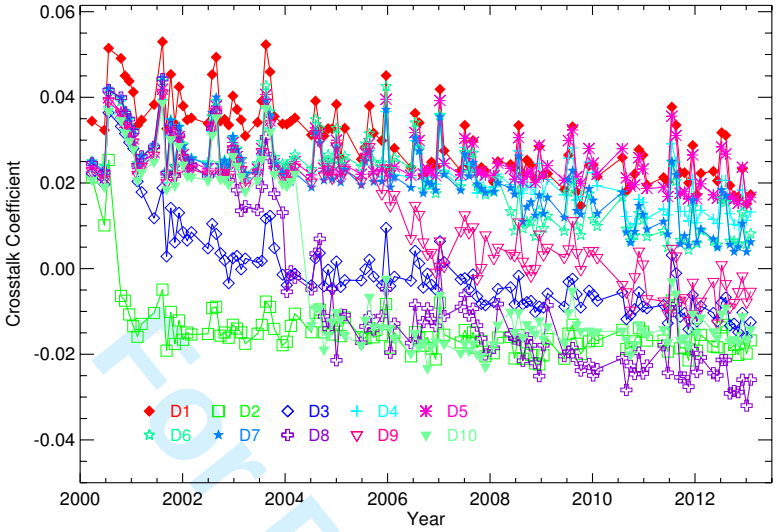

Figure 10, Terra band 28 crosstalk coefficients for sending band 27.

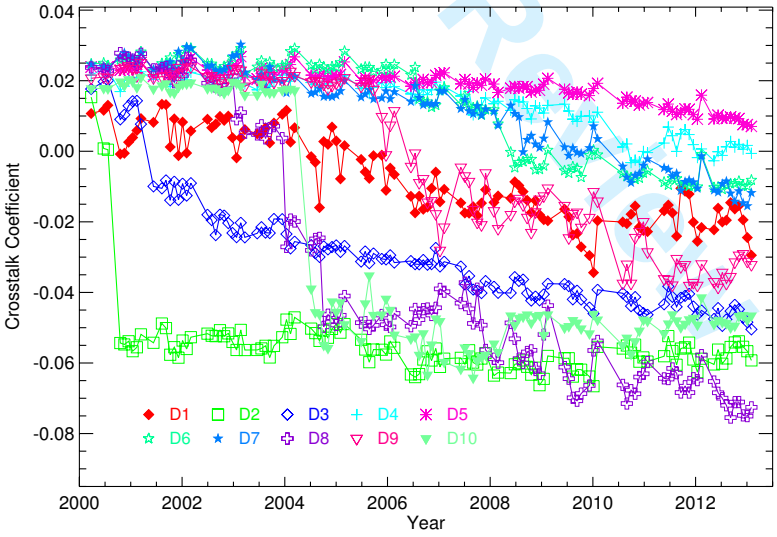

Figure 11, Terra band 28 crosstalk coefficients for sending band 29.

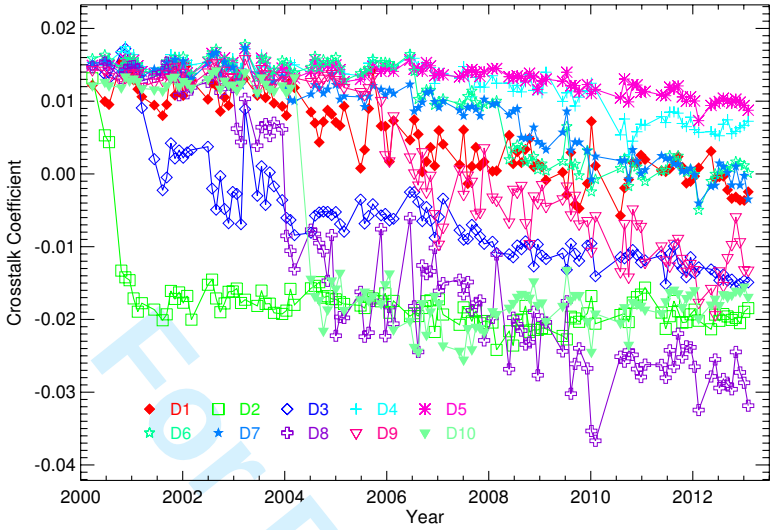

Figure 12, Terra band 28 crosstalk coefficients for sending band 30.

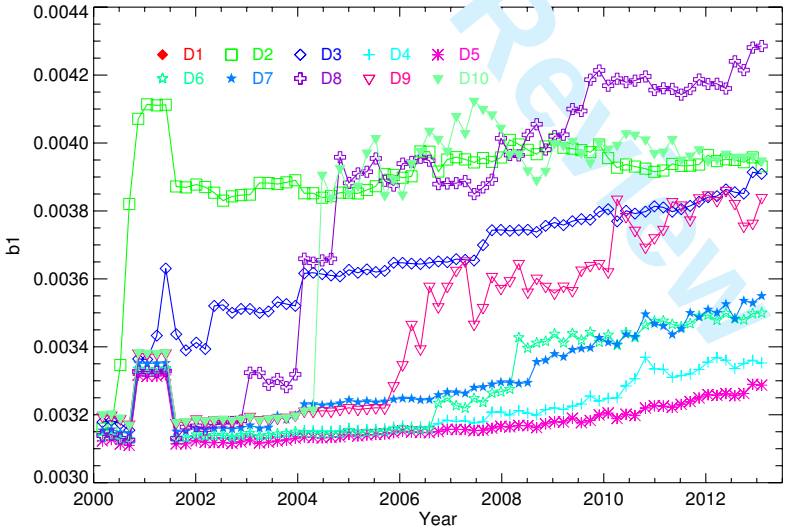

Figure 13, Terra band b1 before correction for individual detectors.

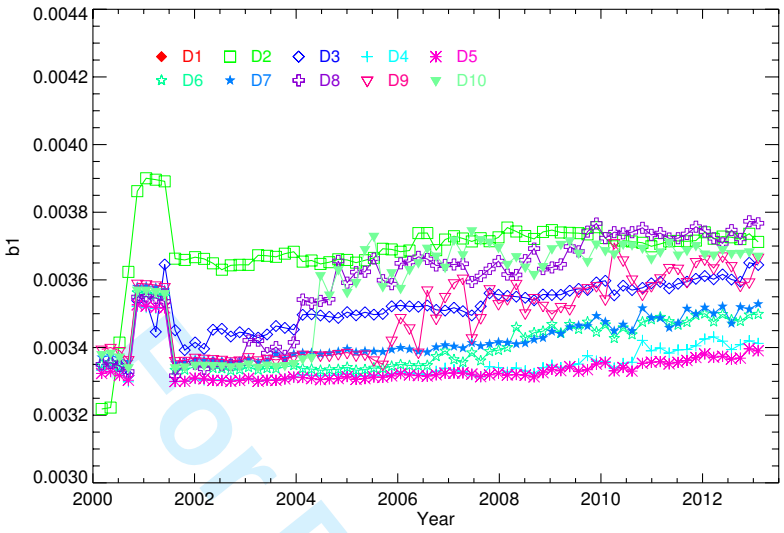

Figure 14, Terra band b1 after correction for individual detectors.

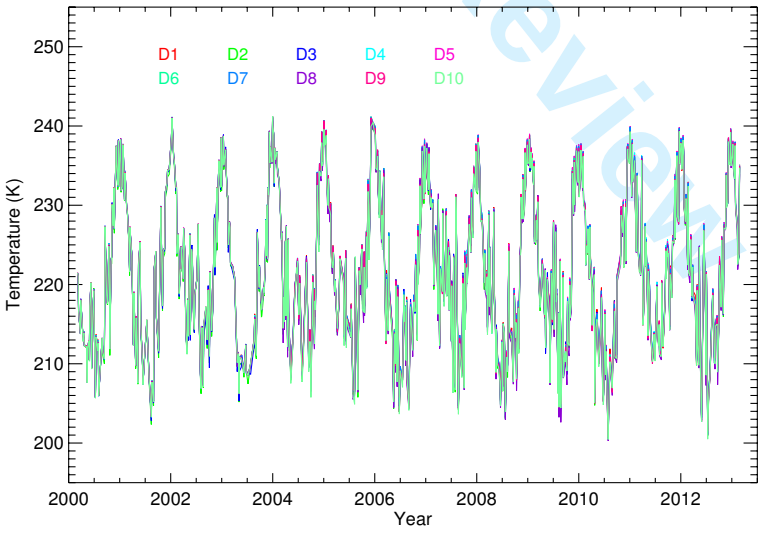

Figure 15, Terra MODIS band 28 C6 brightness temperature at DOME C.

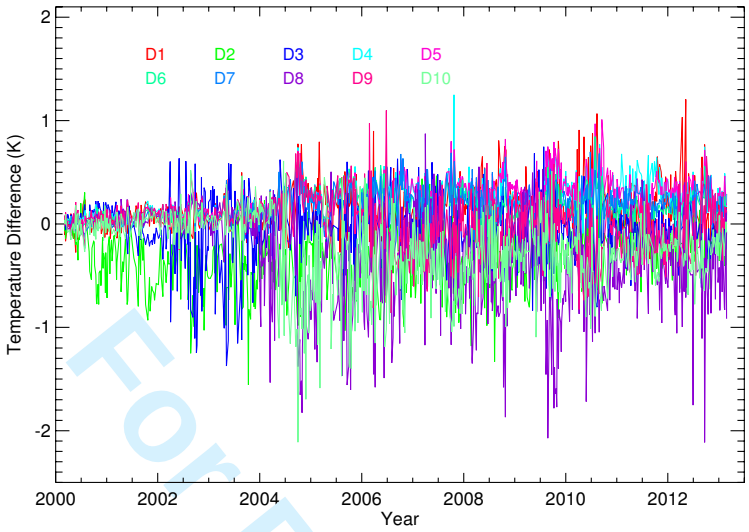

Figure 16, Terra MODIS band 28 C6 brightness temperature detector difference at DOME C.

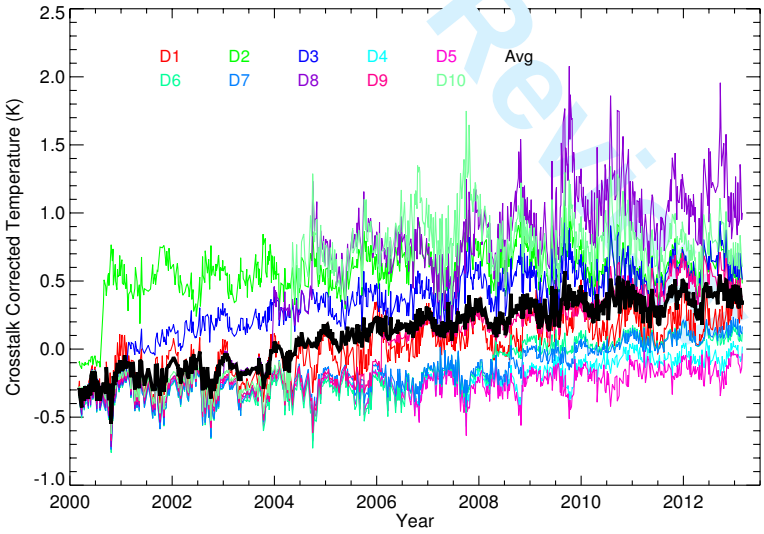

Figure 17, Crosstalk correction for Terra MODIS band 28 C6 brightness temperature at DOME C.

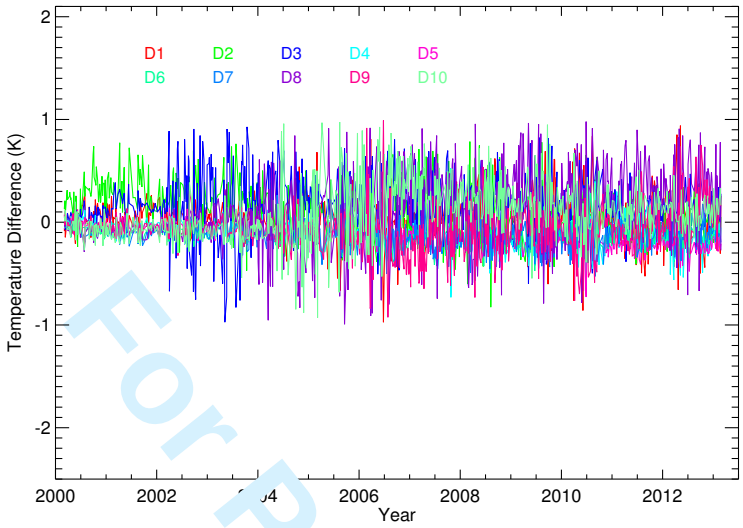

Figure 18, Terra MODIS band 28 C6 brightness temperature detector difference at DOME C after crosstalk correction.

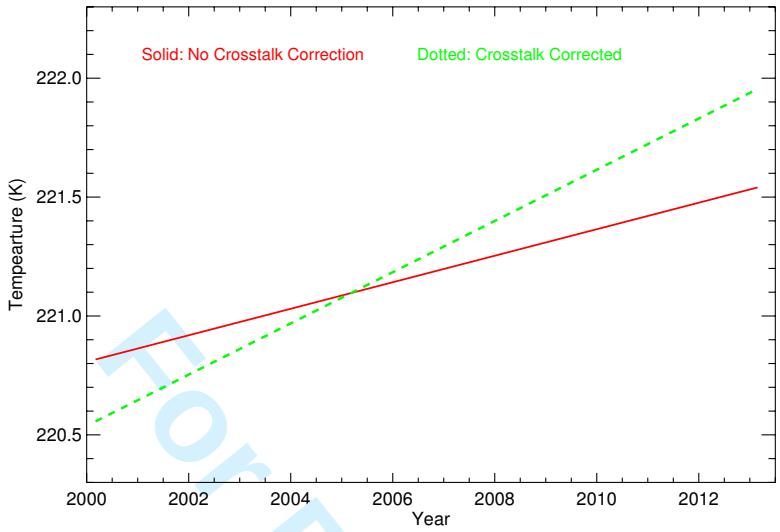

Figure 19, Dome C band averaged BT before (solid) and after (dotted) crosstalk correction.

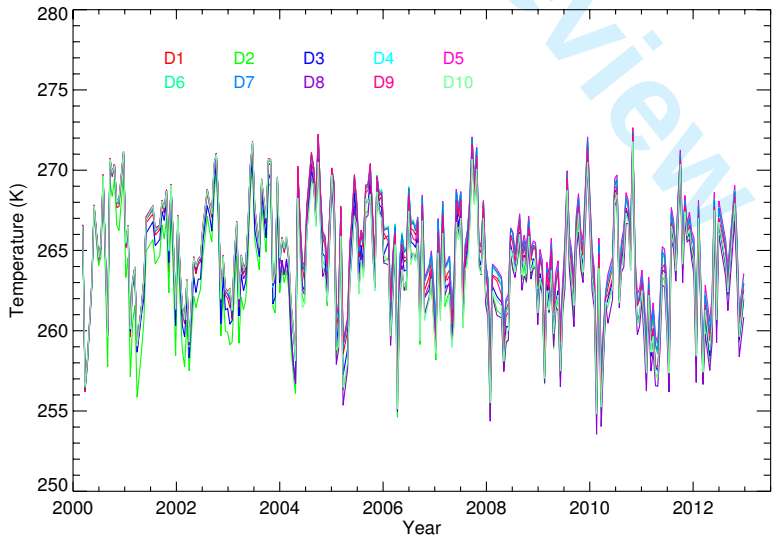

Figure 20, Terra MODIS band 28 C6 brightness temperature at Pacific Ocean.

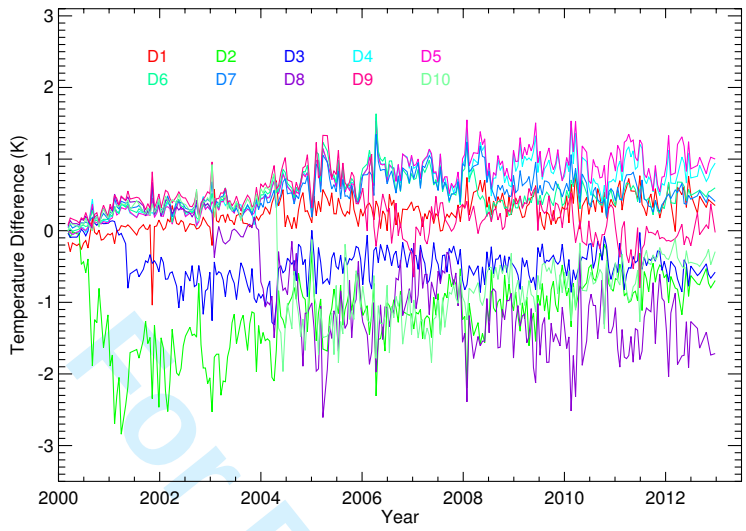

Figure 21, Terra MODIS band 28 C6 brightness temperature detector difference at Pacific Ocean.

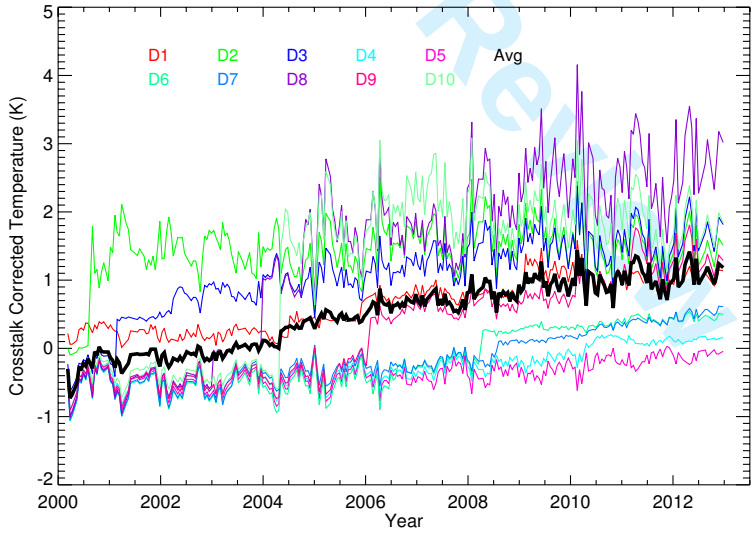

Figure 22, Crosstalk correction for Terra MODIS band 28 C6 brightness temperature at Pacific Ocean.

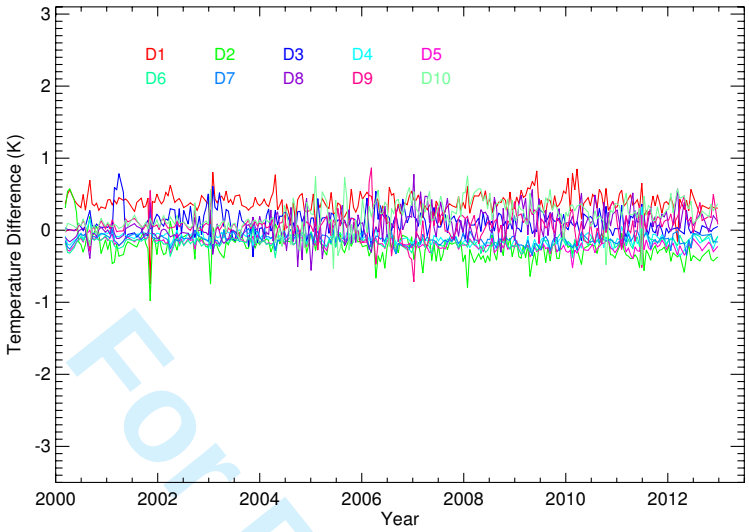

Figure 23, Terra MODIS band 28 C6 brightness temperature detector difference at Pacific Ocean after crosstalk correction.

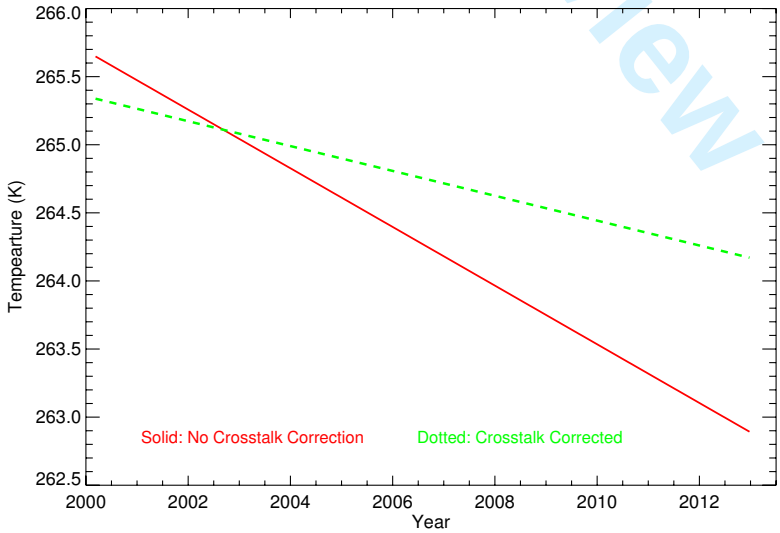

Figure 24, Pacific Ocean band averaged BT before (solid) and after (dotted) crosstalk correction.

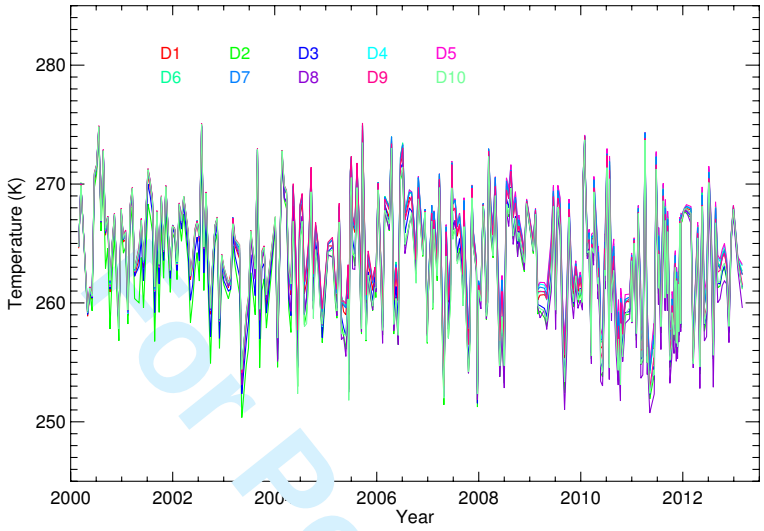

Figure 25, Terra MODIS band 28 C6 brightness temperature at Libya 1.

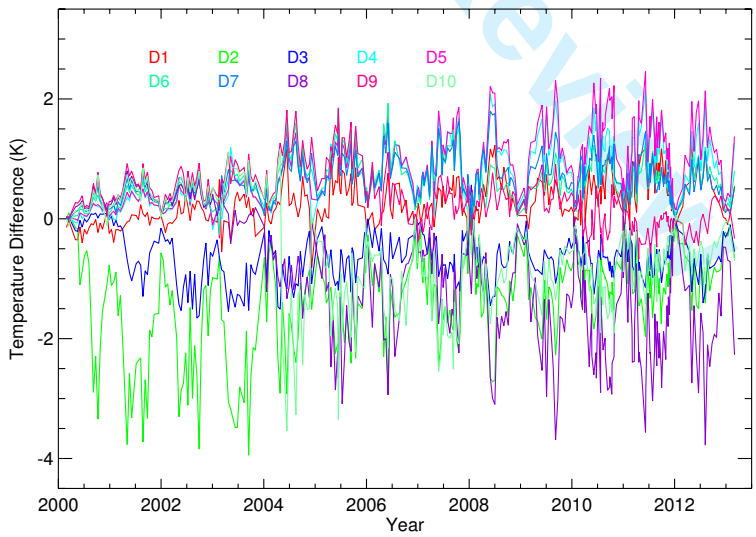

Figure 26, Terra MODIS band 28 C6 brightness temperature detector difference at Libya 1.

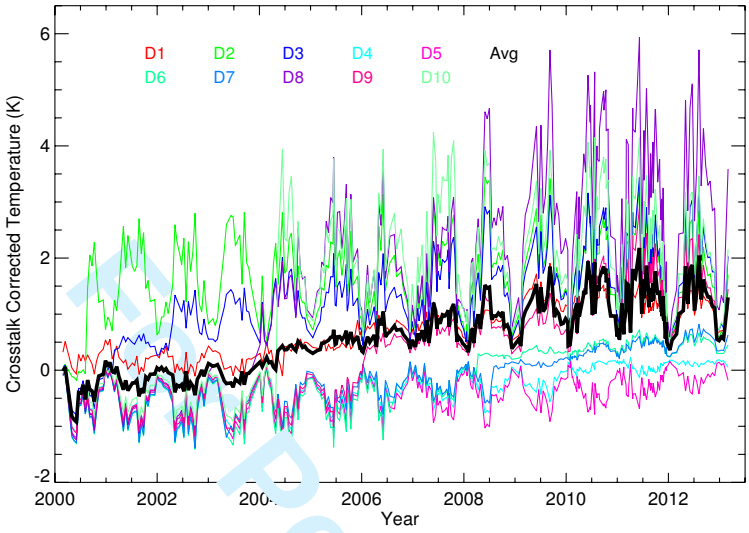

Figure 27, Crosstalk correction for Terra MODIS band 28 C6 brightness temperature at Libya 1.

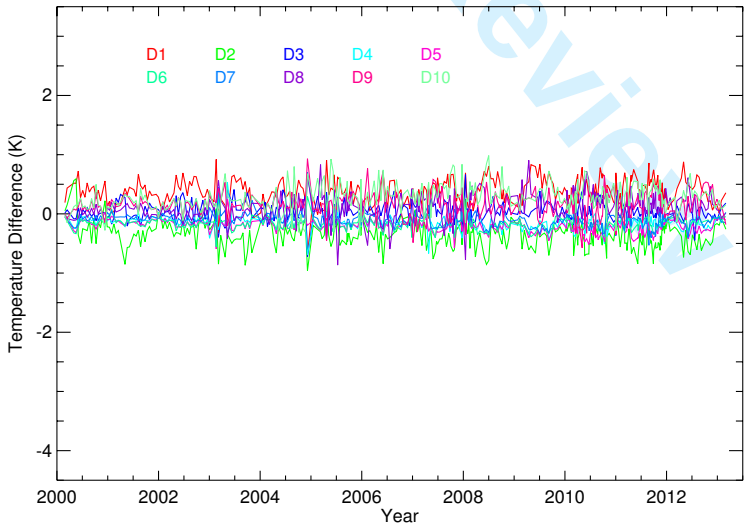

Figure 28, Terra MODIS band 28 C6 brightness temperature detector difference at Libya 1 after crosstalk correction.

Figure 29, Libya 1 band averaged BT before (solid) and after (dotted) crosstalk correction.